Asian Journal of Chemistry; Vol. 27, No. 7 (2015), 2593-2597

ASIAN JOURNAL OF CHEMISTRY

http://dx.doi.org/10.14233/ajchem.2015.18427

Upconversion Properties of $La_2(MoO_4)_3:Er^{3+}/Yb^{3+}$ Green Phosphors Synthesized by Cyclic Microwave-Modified Sol-Gel Method

CHANG SUNG LIM

Department of Advanced Materials Science and Engineering, Hanseo University, Seosan 356-706, Republic of Korea

Corresponding author: Tel/Fax: +82 41 6601445; E-mail: cslim@hanseo.ac.kr

Received: 10 July 2014; *Accepted*: 7 November 2014; *Published online*: 30 March 2015; AJC-17086

Upconversion $La_{2-x}(MoO_4)3:Eu^{3+}/Yb^{3+}$ phosphors with doping concentrations of Er^{3+} and Yb^{3+} ($x = Er^{3+} + Yb^{3+}$, $Er^{3+} = 0.05, 0.1, 0.2$ and $Yb^{3+} = 0.2, 0.45$) were successfully synthesized by the cyclic microwave-assisted sol-gel process and the upconversion photoluminescence properties have been investigated. Well-crystallized particles, formed after heat-treatment at 900 °C for 16 h, showed a fine and homogeneous morphology with particle sizes of 1-5 μm. Under excitation at 980 nm, $La_{1.7}(MoO_4)_3:Er_{0.1}Yb_{0.2}$ and $La_{1.5}(MoO_4)_3:Er_{0.05}Yb_{0.45}$ particles exhibited a strong 525 nm emission band, a weak 550 nm emission band in the green region and a very weak 655 nm emission band in the red region. The Raman spectra of the particles indicated the presence of weak peaks at lower frequencies induced by the disorder of the $[MoO_4]^{2-}$ groups with the incorporation of the Er^{3+} and Yb^{3+} elements into the crystal lattice or by a new phase formation.

Keywords: Upconversion luminescence, Microwave-modified sol-gel, Raman spectroscopy.

INTRODUCTION

Rare earth doped upconversion (UC) phosphors have attracted great attention because of the conversion from near infrared radiation of low energy to visible radiation of high energy. These upconversion photoluminescence particles have potential applications in various fields, including biomedical imaging, owing to their unique upconversion optical behaviors that offer improved light penetration depth, high chemical and photo stability, the absence of auto-fluorescence during imaging, sharp emission bands and high resistance to photobleaching. These properties overcome many of the current limitations in traditional photoluminescence materials[1-3]. It is possible for the structure of the molybdate compounds to be transformed to a highly disordered tetragonal Scheelite structure from the monoclinic structure. It is possible for the trivalent rare earth ions in the disordered tetragonal-phase to be partially substituted by Er^{3+} and Yb^{3+} ions, these ions are effectively doped into the crystal lattices of the tetragonal phase due to the similar radii of the trivalent rare earth ions, this results in the excellent upconversion photoluminescence properties[4-6]. Among rare earth ions, the Er^{3+} ion is suitable for converting infrared to visible light through the upconversion process due to its appropriate electronic energy level configuration. The co-doped Yb^{3+} ion and Er^{3+} ion can remarkably enhance the upconversion efficiency for the shift from infrared to visible light due to the efficiency of the energy transfer from Yb^{3+} to Er^{3+}. The Yb^{3+} ion, as a sensitizer, can be effectively excited by an incident light source energy. This energy is transferred to the activator from which radiation can be emitted. The Er^{3+} ion activator is the luminescence center of the upconversion particles, while the sensitizer enhances the upconversion luminescence efficiency[7-9].

Recently, rare earth activated molybdates have attracted great attention because of their spectroscopic characteristics and excellent upconversion photoluminescence properties. Several processes have been developed to prepare these rare earth doped molybdates, including solid-state reactions[9-14], co-precipitation[15,16], the sol-gel method[4-7], the hydrothermal method[17,18], the Pechini method[19,20], organic gel-thermal decomposition[21] and the microwave-assisted hydrothermal method[22]. For practical application of upconversion photoluminescence in products such as lasers, three-dimensional displays, light-emitting devices and biological detectors, features such as the homogeneous upconversion particle size distribution and morphology need to be well defined. Usually, molybdates are prepared by a solid-state method that requires high temperatures, a lengthy heating process and subsequent grinding, these results in a loss of the emission intensity and an increase in cost. The sol-gel process provides some advantages over the conventional solid-state method, including good homogeneity, low calcination temperature, small particle size and narrow particle size distribution optimal for good luminescent characteristics. However, the sol-gel process has a

disadvantage in that it takes a long time for gelation. Compared with the usual methods, microwave synthesis has the advantages of a very short reaction time, small-size particles, narrow particle size distribution and high purity of final polycrystalline samples. Microwave heating is delivered to the material surface by radiant and/or convection heating, which is transferred to the bulk of the material *via* conduction[23,24]. A cyclic microwave-modified sol-gel process is a cost-effective method that provides high homogeneity and is easy to scale-up and it is emerging as a viable alternative approach for the quick synthesis of high-quality luminescent materials.

In this study, $La_{2-x}(MoO_4)_3:Er^{3+}/Yb^{3+}$ phosphors with doping concentrations of Er^{3+} and Yb^{3+} ($x = Er^{3+} + Yb^{3+}$, Er^{3+} = 0.05, 0.1, 0.2 and Yb^{3+} = 0.2, 0.45) phosphors were prepared *via* the cyclic microwave-modified sol-gel route followed by heat treatment. The synthesized particles were characterized by X-ray diffraction (XRD), scanning electron microscopy (SEM) and energy-dispersive X-ray spectroscopy (EDS). The optical properties were examined comparatively using photoluminescence (PL) emission and Raman spectroscopy.

EXPERIMENTAL

Appropriate stoichiometric amounts of $La(NO_3)_3·6H_2O$ (99 %, Sigma-Aldrich, USA), $(NH_4)_6Mo_7O_{24}·4H_2O$ (99 %, Alfa Aesar, USA), $Er(NO_3)_3·5H_2O$ (99.9 %, Sigma-Aldrich, USA), $Yb(NO_3)_3·5H_2O$ (99.9 %, Sigma-Aldrich, USA), citric acid (99.5 %, Daejung Chemicals, Korea), NH_4OH (A.R.), ethylene glycol (A.R.) and distilled water were used to prepare $La_2(MoO_4)_3$, $La_{1.8}(MoO_4)_3:Er_{0.2}$, $La_{1.7}(MoO_4)_3:Er_{0.1}Yb_{0.2}$ and $La_{1.5}(MoO_4)_3:Er_{0.05}Yb_{0.45}$ compounds with doping concentrations of Er^{3+} and Yb^{3+} (Er^{3+} = 0.05, 0.1, 0.2 and Yb^{3+} = 0.2, 0.45). To prepare $La_2(MoO_4)_3$, 0.4 mol % $La(NO_3)_2·6H_2O$ and 0.4 mol % $(NH_4)_6Mo_7O_{24}·4H_2O$ were dissolved in 20 mL of ethylene glycol and 80 mL of 5M NH_4OH under vigorous stirring and heating. Subsequently, citric acid (with a molar ratio of citric acid to total metal ions of 2:1) was dissolved in 100 mL of distilled water under vigorous stirring and heating. Then, the solutions were mixed together under vigorous stirring and heating at 80-100 °C. At the end, highly transparent solutions were obtained and adjusted to pH = 7-8 by the addition of 8 M NH_4OH or citric acid. In order to prepare $La_{1.8}(MoO_4)_3:Er_{0.2}$, the mixture of 0.72 mol % $La(NO_3)_3·6H_2O$ with 0.08 mol % $Er(NO_3)_3·5H_2O$ was used for the creation of the rare earth solution. In order to prepare $La_{1.7}(MoO_4)_3:Er_{0.1}Yb_{0.2}$, the mixture of 0.68 mol % $La(NO_3)_3·6H_2O$ with 0.04 mol % $Er(NO_3)_3·5H_2O$ and 0.08 mol % $Yb(NO_3)_3·5H_2O$ was used for the creation of the rare earth solution. In order to prepare $La_{1.5}(MoO_4)_3:Er_{0.05}Yb_{0.45}$, the rare earth containing solution was generated using 0.6 mol % $La(NO_3)_3·6H_2O$ with 0.02 mol % $Er(NO_3)_3·5H_2O$ and 0.18 mol % $Yb(NO_3)_3·5H_2O$.

The transparent solutions were placed into a microwave oven operating at a frequency of 2.45 GHz with a maximum output-power of 1250 W for 0.5 h. The working cycle of the microwave reaction was controlled very precisely using a regime of 40 s on and 20 s off for 15 min, followed by further treatment of 30 s on and 30 s off for 15 min. The ethylene glycol was evaporated slowly at its boiling point. Ethylene glycol is a polar solvent at its boiling point of 197 °C, this solvent is a good candidate for the microwave process. If ethylene glycol is used as the solvent, the reactions proceed at the boiling point temperature. When microwave radiation is supplied to the ethylene-glycol-based solution, the components dissolved in the ethylene glycol can couple. The charged particles vibrate in the electric field interdependently when a large amount of microwave radiation is supplied to the ethylene glycol. The samples were treated with ultrasonic radiation for 10 min to produce a light yellow transparent sol. After this, the light yellow transparent sols were dried at 120 °C in a dry oven to obtain black dried gels. The black dried gels were grinded and heat-treated at 900 °C for 16 h with 100 °C intervals between 600-900 °C. Finally, white particles were obtained for $La_2(MoO_4)_3$ and pink particles for $La_{1.8}(MoO_4)_3:Er_{0.2}$, $La_{1.7}(MoO_4)_3:Er_{0.1}Yb_{0.2}$ and $La_{1.5}(MoO_4)_3:Er_{0.05}Yb_{0.45}$ compositions.

The phase composition of the synthesized particles was identified using XRD (D/MAX 2200, Rigaku, Japan). The microstructure and surface morphology of the $La_2(MoO_4)_3$, $La_{1.8}(MoO_4)_3:Er_{0.2}$, $La_{1.7}(MoO_4)_3:Er_{0.1}Yb_{0.2}$ and $La_{1.5}(MoO_4)_3:Er_{0.05}Yb_{0.45}$ particles were observed using SEM/EDS (JSM-5600, JEOL, Japan). The PL spectra were recorded using a spectrophotometer (Perkin Elmer LS55, UK) at room temperature. Raman spectroscopy measurements were performed using a LabRam Aramis (Horiba Jobin-Yvon, France). The 514.5 nm line of an Ar ion laser was used as the excitation source and the power on the samples was kept at 0.5 mW.

RESULTS AND DISCUSSION

Fig. 1 shows the XRD patterns of the (a) JCPDS 46-0407 data of $La_2(MoO_4)_3$, the synthesized (b) $La_2(MoO_4)_3$, (c) $La_{1.8}(MoO_4)_3:Er_{0.2}$, (d) $La_{1.7}(MoO_4)_3:Er_{0.1}Yb_{0.2}$ and (e) $La_{1.5}(MoO_4)_3:Er_{0.05}Yb_{0.45}$ particles. The crystal structures are in good agreement with the crystallographic data of $La_2(MoO_4)_3$ (JCPDS 46-0407). The pure $La_2(MoO_4)_3$ has no impurity phases. Impurity phases were detected at 22°, 23°, 24°, 25°, 29°, 32° and 50° in Fig. 1b-e. The foreign reflexes are marked with an asterisk in Fig. 1e when the doping concentration of Er^{3+}/Yb^{3+} is 0.02/0.18 mol %. A similar impurity phase was also observed in the case of Er^{3+}/Yb^{3+} doped $CaMoO_4$ phosphor when the doping concentration of Er^{3+}/Yb^{3+} is 0.02/0.18 mol %[25]. The foreign reflexes marked with an asterisk in Fig. 1(e) compared to the Er^{3+}/Yb^{3+} doped $CaMoO_4$ can be ascribed to the fact that La^{3+}, Er^{3+} and Yb^{3+} ions are well substituted in the tetragonal-phase $La_{2-x}(MoO_4)_3:Er^{3+}/Yb^{3+}$ of the scheelite-type structure and form a new phase induced by the disorder of the $[MoO_4]^{2-}$ groups[25]. This suggests that the cyclic microwave-modified sol-gel route is suitable for the growth of $La_{2-x}(MoO_4)_3:Er^{3+}/Yb^{3+}$ crystallites. Post heat-treatment plays an important role in a well-defined crystallized morphology. To achieve a well-defined crystalline morphology, $La_2(MoO_4)_3$, $CaLa_{1.8}(MoO_4)_3:Er_{0.2}$, $CaLa_{1.7}(MoO_4)_3:Er_{0.1}Yb_{0.2}$ and $CaLa_{1.5}(MoO_4)_3:Er_{0.05}Yb_{0.45}$ phases need to be heat treated at 900 °C for 16 h. It is assumed that the doping amount of Er^{3+}/Yb^{3+} has a great effect on the crystalline cell volume of the $La_2(MoO_4)_3$, because of the different ionic sizes and energy band gaps. This means that the obtained samples possess a tetragonal-phase after partial substitution of La^{3+} by Er^{3+} and

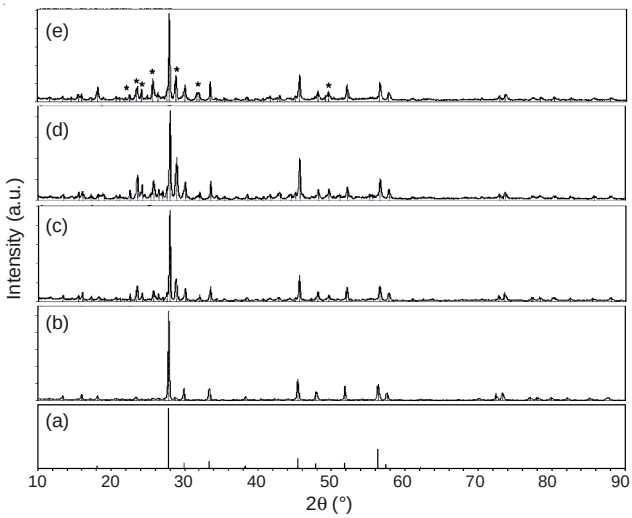

Fig. 1. X-ray diffraction patterns of the (a) JCPDS 46-0407 data of $La_2(MoO_4)_3$, the synthesized (b) $La_2(MoO_4)_3$, (c) $La_{1.8}(MoO_4)_3:Er_{0.2}$, (d) $La_{1.7}(MoO_4)_3:Er_{0.1}Yb_{0.2}$, and (e) $La_{1.5}(MoO_4)_3:Er_{0.05}Yb_{0.45}$ particles

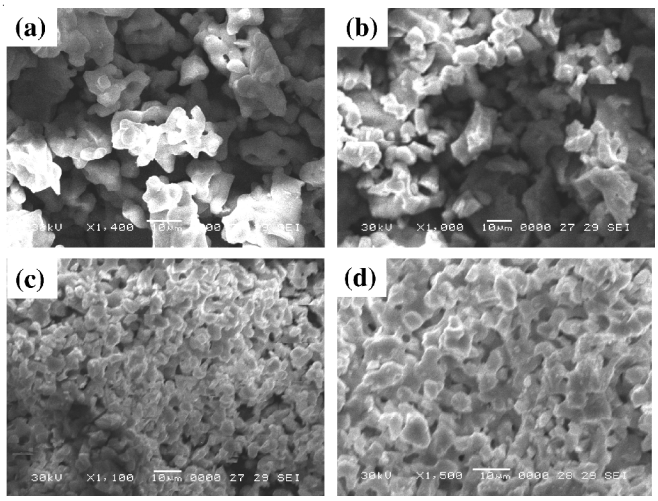

Fig. 2. Scanning electron microscopy images of the synthesized (a) $La_2(MoO_4)_3$, (b) $La_{1.8}(MoO_4)_3:Er_{0.2}$, (c) $La_{1.7}(MoO_4)_3:Er_{0.1}Yb_{0.2}$, and (d) $La_{1.5}(MoO_4)_3:Er_{0.05}Yb_{0.45}$ particles

Yb^{3+} ions and the ions are effectively doped into crystal lattices of the $La_2(MoO_4)_3$ phase due to the similar radii of La^{3+}, Er^{3+} and Yb^{3+}.

Fig. 2 shows SEM images of the synthesized (a) $La_2(Mo\text{-}O_4)_3$, (b) $La_{1.8}(MoO_4)_3:Er_{0.2}$, (c) $La_{1.7}(MoO_4)_3:Er_{0.1}Yb_{0.2}$ and (d) $La_{1.5}(MoO_4)_3:Er_{0.05}Yb_{0.45}$ particles. The as-synthesized samples are well crystallized with a fine and homogeneous morphology and particle size of 1-5 μm. The sample of (a) $La_2(MoO_4)_3$ shows a well crystallized morphology with a particle size of 1-5 μm. The samples of (c) $La_{1.7}(MoO_4)_3:Er_{0.1}Yb_{0.2}$ and (d) $La_{1.5}(MoO_4)_3:Er_{0.05}Yb_{0.45}$ have some agglomerated particles compared to the sample of (a) $La_2(MoO_4)_3$. It should be noted that the doping amounts for Er^{3+} and Yb^{3+} have a great effect on the morphological features. Fig. 3 shows the (a) energy-dispersive X-ray spectroscopy patterns, (b) quantitative compositions and (c) quantitative results of the synthesized $La_{1.5}(MoO_4)_3:Er_{0.05}Yb_{0.45}$ particles. The EDS pattern (a) shows that the $La_{1.5}(MoO_4)_3:Er_{0.05}Yb_{0.45}$ particles are composed of La, Mo, O, Er and Yb. The quantitative compositions (b) show precise constitutions of the synthesized $La_{1.5}(MoO_4)_3:Er_{0.05}Yb_{0.45}$ particles. The quantitative results (c) are in good relation with a nominal composition of the $La_{1.5}(MoO_4)_3:Er_{0.05}Yb_{0.45}$ particles. The relations between La, Mo, O, Er and Yb show that the $La_{1.5}(MoO_4)_3:Er_{0.05}Yb_{0.45}$ particles can be successfully synthesized using the cyclic microwave-modified sol-gel method. The cyclic microwave-modified sol-gel process of molybdates provides the energy to synthesize the bulk of the material uniformly, so that fine particles with controlled morphology can be fabricated in a short time period. The method is a cost-effective way to provide highly homogeneous products and is easy to scale-up, it is a viable alternative for the rapid synthesis of upconversion particles.

Fig. 4 shows the upconversion photoluminescence emission spectra of the as-prepared (a) $La_2(MoO_4)_3$, (b) $La_{1.8}(MoO_4)_3:Er_{0.2}$, (c) $La_{1.7}(MoO_4)_3:Er_{0.1}Yb_{0.2}$ and (d) $La_{1.5}(MoO_4)_3:Er_{0.05}Yb_{0.45}$ particles excited under 980 nm at room temperature. The upconversion intensities of (c) $La_{1.7}(MoO_4)_3:Er_{0.1}Yb_{0.2}$ and (d) $La_{1.5}(MoO_4)_3:Er_{0.05}Yb_{0.45}$ particles exhibited a strong 525 nm emission band, a weak 550 nm emission band in the green region and a very weak 655 nm emission band in the red region. The strong 525 nm emission band and the weak 550 nm emission band in the green region correspond to the

(a)

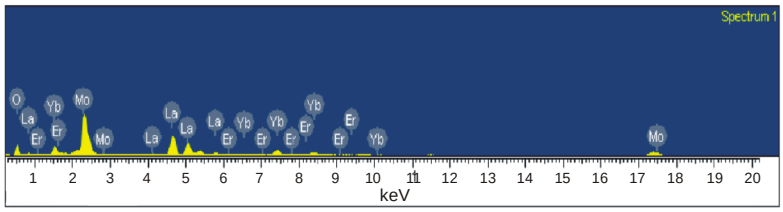

(b)

Spectrum	In stats.	0	Mo	La	Er	Yb	Total
Spectrum1	Yes	25.03	31.95	27.07	0.43	15.53	100.00
Spectrum2	Yes	25.97	32.23	27.02	0.81	13.97	100.00
Spectrum3	Yes	24.24	32.06	26.56	0.48	16.66	100.00
Spectrum4	Yes	24.48	32.63	26.70	0.55	15.64	100.00
Mean		24.93	32.22	26.84	0.56	15.45	100.00
Std. deviation		0.77	0.30	0.25	0.17	1.11	
Max.		25.97	32.63	27.07	0.81	16.66	
Min.		24.24	31.95	26.56	0.43	13.97	

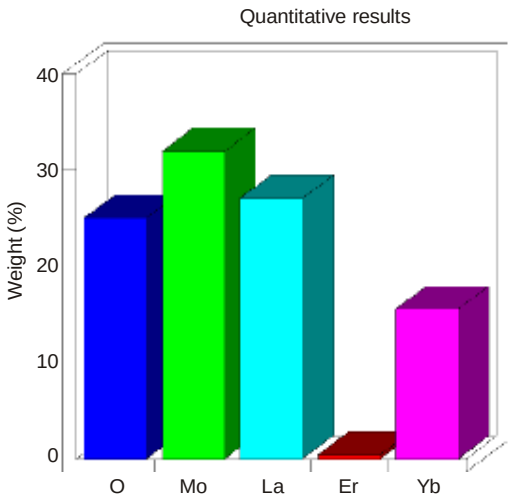

Fig. 3. Energy-dispersive X-ray spectroscopy patterns (a), quantitative compositions (b) and quantitative results (c) of the synthesized $La_{1.5}(MoO_4)_3:Er_{0.05}Yb_{0.45}$ particles

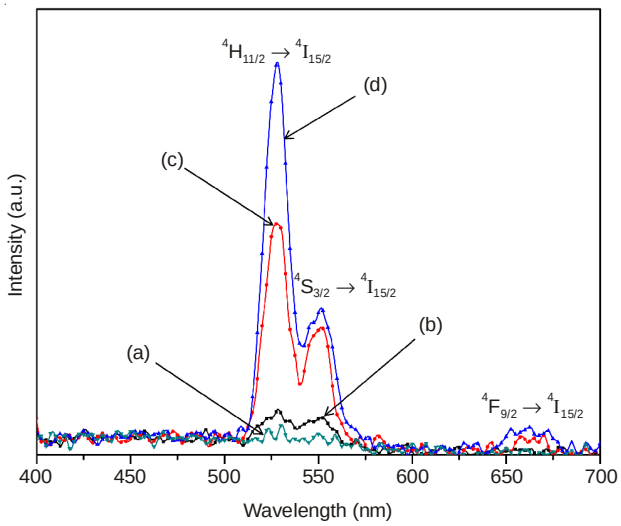

Fig. 4. Upconversion photoluminescence emission spectra of (a) $La_2(MoO_4)_3$, (b) $La_{1.8}(MoO_4)_3$:$Er_{0.2}$, (c) $La_{1.7}(MoO_4)_3$:$Er_{0.1}Yb_{0.2}$, and (d) $La_{1.5}(Mo\text{-}O_4)_3$:$Er_{0.05}Yb_{0.45}$ particles excited under 980 nm at room temperature

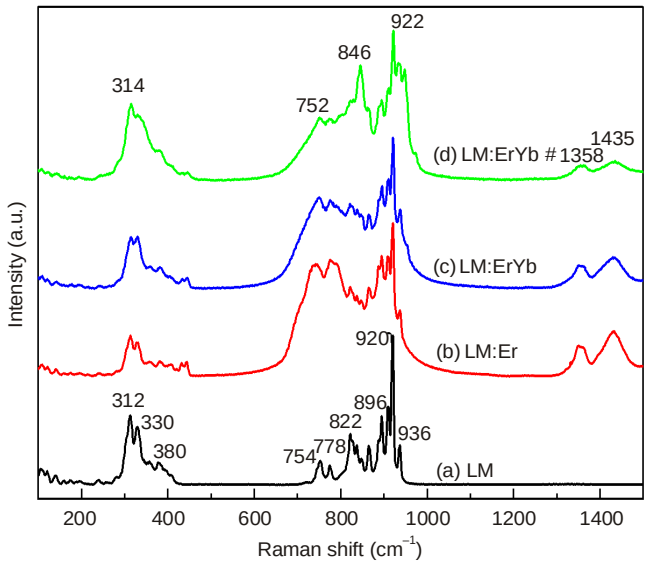

Fig. 5. Raman spectra of the synthesized (a) $La_2(MoO_4)_3$(LM), (b) $La_{1.8}(MoO_4)_3$:$Er_{0.2}$(LM:Er), (c) $La_{1.7}(MoO_4)_3$:$Er_{0.1}Yb_{0.2}$(LM:ErYb) and (d) $La_{1.5}(MoO_4)_3$:$Er_{0.05}Yb_{0.45}$(LM:ErYb#) particles excited by the 514.5 nm line of an Ar ion laser at 0.5 mW

$^2H_{11/2} \rightarrow {}^4I_{15/2}$ and $^4S_{3/2} \rightarrow {}^4I_{15/2}$ transitions, respectively, while the very weak emission 655 nm band in the red region corresponds to the $^4F_{9/2} \rightarrow {}^4I_{15/2}$ transition. The upconversion intensities of (a) $La_2(MoO_4)_3$ was not detected. The upconversion intensity of (d) $La_{1.5}(MoO_4)_3$:$Er_{0.05}Yb_{0.45}$ is much higher than those of (b) $La_{1.8}(MoO_4)_3$:$Er_{0.2}$ and (c) $La_{1.7}(MoO_4)_3$:$Er_{0.1}Yb_{0.2}$ particles. Similar results are also observed from Er^{3+}/Yb^{3+} co-doped in other host matrices, which are assigned to the upconversion emission spectra with the green emission intensity ($^2H_{11/2} \rightarrow {}^4I_{15/2}$ and $^4S_{3/2} \rightarrow {}^4I_{15/2}$ transitions) and the red emission intensity ($^4F_{9/2} \rightarrow {}^4I_{15/2}$ transition)[7,10,25-27]. The doping amounts of Er^{3+}/Yb^{3+} had a great effect on the morphological features of the particles and their upconversion fluorescence intensity. The Yb^{3+} ion sensitizer can be effectively excited by the energy of an incident light source, this energy is transferred to the activator where radiation can be emitted. The Er^{3+} ion activator is the luminescence center for these upconversion particles and the sensitizer enhances the upconversion luminescence efficiency. The upconversion process is a proven method for generating visible light from near infrared (NIR) radiation. upconversion is a nonlinear optical process in which excitation of the lower electronic levels with low-energy radiation (NIR light) results in higher energy emission (visible or ultraviolet light) at higher electronic levels; thus, it is ascribed as an anti-Stockes mechanism. This process requires the absorption of two or more photons to produce sufficient energy for upconversion emission. The much higher intensity of the $^2H_{11/2} \rightarrow {}^4I_{15/2}$ transition in comparison with the $^4S_{3/2} \rightarrow {}^4I_{15/2}$ transition in Fig. 4 may be induced by the concentration quenching effect due to the energy transfer between the nearest Er^{3+} and Yb^{3+} ions and the interactions between doping ions in the $La_{2-x}(MoO_4)_3$ host matrix. This means that the green band $^2H_{11/2} \rightarrow {}^4I_{15/2}$ transitions are assumed to be more easily quenched than the $^4S_{3/2} \rightarrow {}^4I_{15/2}$ transition by non-radiative relaxation in the case of the host matrix.

Fig. 5 shows the Raman spectra of the synthesized (a) $La_2(MoO_4)_3$ (LM), (b) $La_{1.8}(MoO_4)_3$:$Er_{0.2}$(LM:Er), (c) $La_{1.7}(MoO_4)_3$:$Er_{0.1}Yb_{0.2}$(LM:ErYb) and (d) $La_{1.5}(MoO_4)_3$:$Er_{0.05}Yb_{0.45}$ (LM:ErYb#) particles excited by the 514.5 nm line of an Ar ion laser at 0.5 mW. The internal modes for the (a) $La_2(MoO_4)_3$ (LM) particles were detected at 312, 330, 380, 754, 778, 822, 896, 920 and 936 cm^{-1}, respectively. The well-resolved sharp peaks for the $La_2(MoO_4)_3$ particles indicate a high crystallinity state of the synthesized particles. The internal vibration mode frequencies are dependent on the lattice parameters and the degree of the partially covalent bond between the cation and molecular ionic group $[MoO_4]^{2-}$. The Raman spectra of the (b) $La_{1.8}(MoO_4)_3$:$Er_{0.2}$ (LM:Er), (c) $La_{1.7}(MoO_4)_3$:$Er_{0.1}Yb_{0.2}$ (LM:ErYb) and (d) $La_{1.5}(MoO_4)_3$:$Er_{0.05}Yb_{0.45}$ (LM:ErYb#) particles indicate the weak peaks at lower frequencies (1358 and 1435 cm^{-1}). The Raman spectra of (b) $La_{1.8}(MoO_4)_3$:$Er_{0.2}$(LM:Er), (c) $La_{1.7}(MoO_4)_3$:$Er_{0.1}Yb_{0.2}$(LM:ErYb) and (d) $La_{1.5}(MoO_4)_3$:$Er_{0.05}Yb_{0.45}$(LM:ErYb#) particles prove that the doping ions can influence the structure of the host materials. The combination of a heavy metal cation and the large inter-ionic distance for Er^{3+} and Yb^{3+} substitutions in La^{3+} sites in the lattice result in a low probability of upconversion and phonon-splitting relaxation in $La_{2-x}(MoO_4)_3$ crystals. It may be that these very strong and strange effects are generated by the disorder of the $[MoO_4]^{2-}$ groups with the incorporation of the Er^{3+} and Yb^{3+} elements into the crystal lattice or by a new phase formation.

Conclusion

The $La_{2-x}(MoO_4)_3$:Er^{3+}/Yb^{3+} phosphors with doping concentrations of Er^{3+} and Yb^{3+} (x = Er^{3+} + Yb^{3+}, Er^{3+} = 0.05, 0.1, 0.2 and Yb^{3+} = 0.2, 0.45) were successfully synthesized by the cyclic microwave-modified sol-gel method. Well-crystallized particles formed after heat-treatment at 900 °C for 16 h showed a fine and homogeneous morphology with particle sizes of 1-5 μm. Under excitation at 980 nm, the upconversion intensities of $La_{1.7}(MoO_4)_3$:$Er_{0.1}Yb_{0.2}$ and $La_{1.5}(MoO_4)_3$:$Er_{0.05}Yb_{0.45}$ particles exhibited a strong 525 nm emission band and a weak 550 nm emission band in the green region, which were assigned to the $^2H_{11/2} \rightarrow {}^4I_{15/2}$ and $^4S_{3/2} \rightarrow {}^4I_{15/2}$ transitions, respectively, while a very weak 655 nm emission band in the red region was assigned to the $^4F_{9/2} \rightarrow$

$^4I_{15/2}$ transition. The upconversion intensity of $La_{1.5}(MoO_4)_3:Er_{0.05}Yb_{0.45}$ particles was much higher than that of the $La_{1.8}(MoO_4)_3:Er_{0.2}$ and $La_{1.7}(MoO_4)_3:Er_{0.1}Yb_{0.2}$ particles. The Raman spectra of the $La_{1.8}(MoO_4)_3:Er_{0.2}$, $La_{1.7}(MoO_4)_3:Er_{0.1}Yb_{0.2}$ and $La_{1.5}(MoO_4)_3:Er_{0.05}Yb_{0.45}$ particles indicated the weak peaks at lower frequencies (1358 and 1435 cm^{-1}) induced by the disorder of the $[MoO_4]^{2-}$ groups with the incorporation of the Er^{3+} and Yb^{3+} elements into the crystal lattice or by a new phase formation.

ACKNOWLEDGEMENTS

This study was supported by the Basic Science Research Program through the National Research Foundation of Korea (NRF) funded the Ministry of Science, ICT & Future Planning (2014-046024).

REFERENCES

1. M. Wang, G. Abbineni, A. Clevenger, C. Mao and S. Xu, *Nanomedicine*, **7**, 710 (2011).
2. Y.J. Chen, H.M. Zhu, Y.F. Lin, X.H. Gong, Z.D. Luo and Y.D. Huang, *Opt. Mater*., **35**, 1422 (2013).
3. M. Lin, Y. Zhao, S.Q. Wang, M. Liu, Z.F. Duan, Y.M. Chen, F. Li, F. Xu and T.J. Lu, *Bio. Adv*, **30**, 1551 (2012).
4. J. Liao, D. Zhou, B. Yang, R. Liu, Q. Zhang and Q. Zhou, *J. Lumin*., **134**, 533 (2013).
5. J. Sun, J. Xian and H. Du, *J. Phys. Chem. Solids*, **72**, 207 (2011).
6. C. Guo, H.K. Yang and J.H. Jeong, *J. Lumin*., **130**, 1390 (2010).
7. T. Li, C. Guo, Y. Wu, L. Li and J.H. Jeong, *J. Alloys Comp*., **540**, 107 (2012).
8. M. Nazarov and D.Y. Noh, *J. Rare Earths*, **28**, 1 (2010).
9. J. Sun, W. Zhang, W. Zhang and H. Du, *Mater. Res. Bull*., **47**, 786 (2012).
10. H. Du, Y. Lan, Z. Xia and J. Sun, *Mater. Res. Bull*., **44**, 1660 (2009).
12. M. Haque and D.K. Kim, *Mater. Lett*., **63**, 793 (2009).
13. C. Zhao, X. Yin, F. Huang and Y. Hang, *J. Solid State Chem*., **184**, 3190 (2011).
14. L. Qin, Y. Huang, T. Tsuboi and H.J. Seo, *Mater. Res. Bull*., **47**, 4498 (2012).
15. Y. Yang, E. Liu, L. Li, Z. Huang, H. Shen and X. Xiang, *J. Alloys Comp*., **505**, 555 (2010).
16. Y. Tian, B. Chen, B. Tian, R. Hua, J. Sun, L. Cheng, H. Zhong, X. Li, J. Zhang, Y. Zheng, T. Yu, L. Huang and Q. Meng, *J. Alloys Comp*., **509**, 6096 (2011).
17. Y. Huang, L. Zhou, L. Yang and Z. Tang, *Opt. Mater*., **33**, 777 (2011).
18. Y. Tian, B. Chen, B. Tian, J. Sun, X. Li, J. Zhang, L. Cheng, H. Zhong, H. Zhong, Q. Meng and R. Hua, *Physica B*, **407**, 2556 (2012).
19. Z. Wang, H. Liang, L. Zhou, J. Wang, M. Gong and Q. Su, *J. Lumin*., **128**, 147 (2008).
20. Q. Chen, L. Qin, Z. Feng, R. Ge, X. Zhao and H. Xu, *J. Rare Earths*, **29**, 843 (2011).
21. X. Shen, L. Li, F. He, X. Meng and F. Song, *Mater. Chem. Phys*., **132**, 471 (2012).
22. J. Zhang, X. Wang, X. Zhang, X. Zhao, X. Liu and L. Peng, *Inorg. Chem. Commun*., **14**, 1723 (2011).
23. S. Das, A.K. Mukhopadhyay, S. Datta and D. Basu, *Bull. Mater. Sci*., **32**, 1 (2009).
24. Y. Keereeta, T. Thongtem and S. Thongtem, *Curr. Appl. Phys*., **12**, S139 (2012).
25. C.S. Lim, *Mater. Res. Bull*., **47**, 4220 (2012).
26. W. Lu, L. Cheng, J. Sun, H. Zhong, X. Li, Y. Tian, J. Wan, Y. Zheng, L. Huang, T. Yu, H. Yu and B. Chen, *Physica B*, **405**, 3284 (2010).
27. J. Sun, J. Xian, X. Zhang and H. Du, *J. Rare Earths*, **29**, 32 (2011).